Retinal Nerve Fiber Layer Imaging with Spectral-Domain Optical Coherence Tomography: Interpreting the RNFL Maps in Healthy Myopic Eyes

Christopher Kai-Shun Leung,[1] *Marco Yu,*[1] *Robert N. Weinreb,*[2] *Heather Kayew Mak,*[1] *Gilda Lai,*[1] *Cong Ye,*[1] *and Dennis Shun-Chiu Lam*[1]

Purpose. To investigate the association between the distribution profile of the retinal nerve fiber layer (RNFL) bundles and myopia and its impact on interpretation of the RNFL map imaged by a spectral-domain optical coherence tomography (SD-OCT).

Methods. The RNFL of 189 myopic eyes from 103 normal healthy myopic participants was imaged by an SD-OCT. The angle between the long axes of the superotemporal and inferotemporal RNFL bundles determined in the RNFL thickness map (the RNFL distribution angle) and the abnormal area in the RNFL thickness deviation map were measured. The associations between the RNFL distribution angle and the axial length/spherical error, and between the area of abnormal RNFL measurement and each of the following: axial length, spherical error, RNFL distribution angle, average RNFL thickness, optic disc area, and signal strength were analyzed with linear mixed models.

Results. The RNFL distribution angle decreased with the axial length ($P < 0.011$). In the univariate analysis, the area of abnormal RNFL measurement was positively associated with the axial length ($P = 0.001$); and negatively associated with the RNFL distribution angle ($P < 0.001$), average RNFL thickness ($P < 0.001$), optic disc area ($P \leq 0.001$), and signal strength ($P = 0.026$). In the multivariate analysis, the area of abnormal RNFL measurement was negatively associated with the RNFL distribution angle independent of other covariates.

Conclusions. The superotemporal and inferotemporal RNFL bundles converged temporally with increasing myopia, which was associated with an increase in area of abnormal RNFL measurement. The interpretation of the RNFL thickness map in myopic eyes requires careful consideration of the distribution pattern of the RNFL bundles. (*Invest Ophthalmol Vis Sci.* 2012; 53:7194–7200) DOI:10.1167/iovs.12-9726

From the [1]Department of Ophthalmology and Visual Sciences, The Chinese University of Hong Kong, Hong Kong, People's Republic of China; and the [2]Hamilton Glaucoma Center and Department of Ophthalmology, University of California, San Diego, La Jolla, California.

Supported by an unrestricted grant from Research to Prevent Blindness (New York, New York).

Submitted for publication February 19, 2012; revised July 21 and September 10, 2012; accepted September 13, 2012.

Disclosure: **C.K.-S. Leung**, Alcon (F), Optovue (F), Carl Zeiss Meditec (F, R), Heidelberg Engineering (R); **M. Yu**, None; **R.N. Weinreb**, Carl Zeiss Meditec (F, C), Optovue (F, C), Topcon (F), Nidek (F), Heidelberg Engineering (F); **H.K. Mak**, None; **G. Lai**, None; **C. Ye**, None; **D.S.-C. Lam**, None

Corresponding author: Christopher Kai-Shun Leung, Department of Ophthalmology and Visual Sciences, The Chinese University of Hong Kong, Hong Kong, People's Republic of China; tlims00@hotmail.com.

The advent of the spectral-domain optical coherence tomography (SD-OCT) for three-dimensional imaging of the retinal nerve fiber layer (RNFL) has provided an objective approach to visualize and quantify the distribution pattern of RNFL defects.[1–4] In a previous study, we introduced a scoring system to analyze the RNFL thickness deviation map obtained with an SD-OCT (Cirrus HD-OCT; Carl Zeiss Meditec, Dublin, CA) to detect glaucomatous RNFL defects.[3] The RNFL thickness deviation map is composed of 50 × 50 pixels representing an area of 6 × 6 mm^2 in the optic disc region. With reference to a normative database, each pixel would be encoded in yellow or red if the RNFL measurement falls below the lower 95% and 99% of the centile ranges, respectively. By analyzing the defect size, shape, depth, location, and distance from the disc margin, we showed that the map analysis outperformed the conventional circumpapillary RNFL measurement in discriminating glaucomatous from normal eyes with high sensitivity and specificity.[3]

As the normative database of the Cirrus HD-OCT (Carl Zeiss Meditec) largely comprises data collected from normal eyes with no or low myopia, interpreting the RNFL thickness deviation map in eyes with moderate to high myopia can be problematic. Myopic eyes have thinner RNFL measurements and may lead to abnormal diagnostic classification.[5–10] Studying the OCT RNFL thickness map generated from the SD-OCT, we observed that the presence of myopia not only impacted the RNFL thickness, but also the distribution pattern of the RNFL bundles. With increasing myopia, the superotemporal and inferotemporal RNFL bundles tend to converge temporally, reducing the angle bounded by them (Fig. 1). We hypothesize that the RNFL distribution angle decreases with the axial length and relates to the area encoded as abnormal in the RNFL thickness deviation map. In this study, we measured the angle between the superotemporal and inferotemporal RNFL bundles in the RNFL thickness map and the area of abnormal pixels classified as "borderline" or "outside normal limits" in the RNFL thickness deviation map with the objectives of investigating the RNFL distribution pattern in myopic eyes and its influence on the interpretation of the RNFL thickness deviation map.

Methods

Subjects

A total of 103 healthy myopic participants with spherical error ≤ −0.5 diopters (D) were consecutively enrolled and included in the analysis. They were followed up during the period from November 2010 to September 2011 at the University Eye Center, the Chinese University of Hong Kong. All subjects underwent a full ophthalmic examination including measurement of visual acuity, refraction and intraocular

Investigative Ophthalmology & Visual Science, October 2012, Vol. 53, No. 11

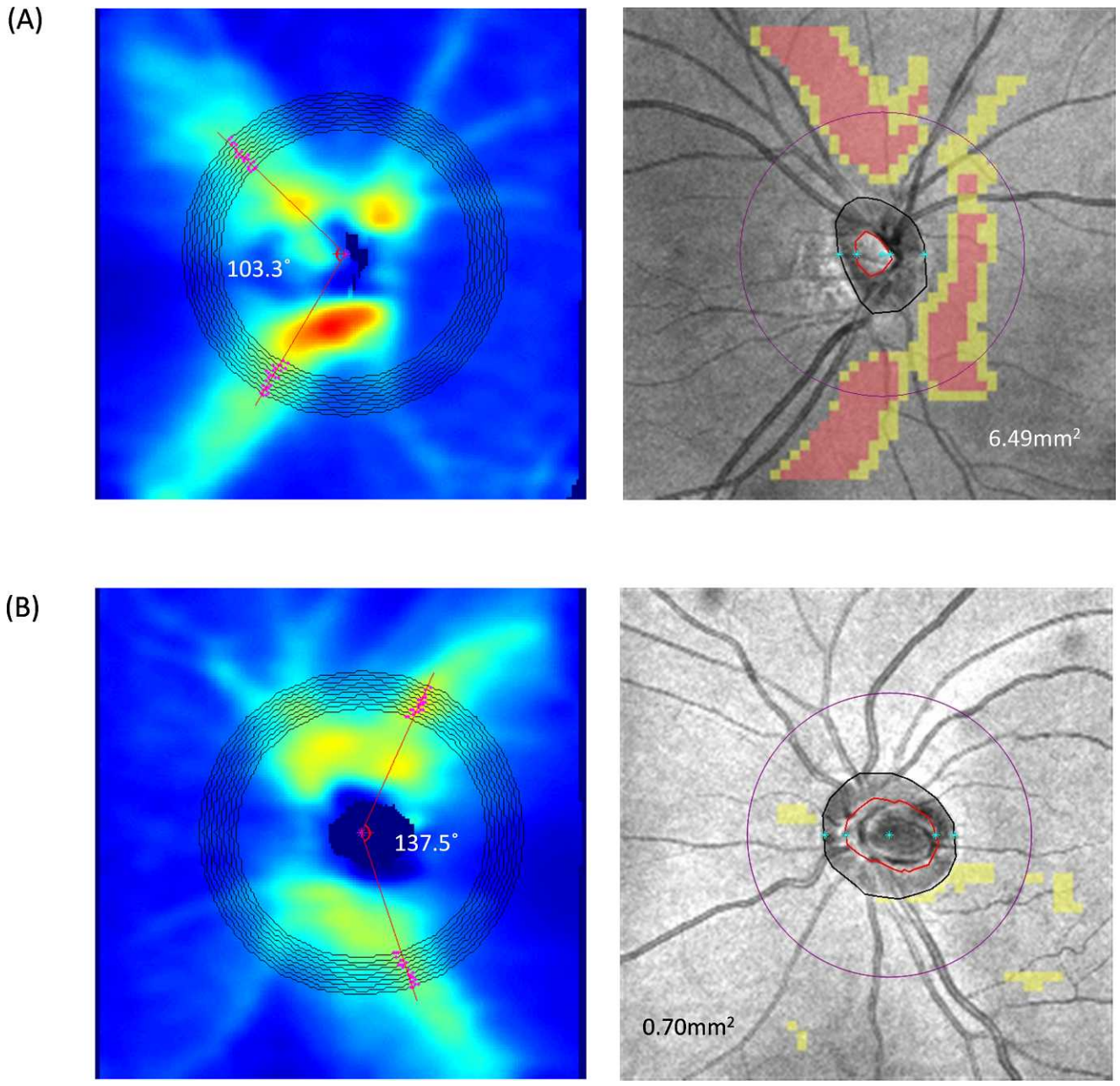

Figure 1. The RNFL thickness maps (*left panel*) and the RNFL thickness deviation maps (*right panel*) of two myopic eyes with axial length of (**A**) 27.26 mm (spherical error: –6.75 D) and (**B**) 26.61 mm (spherical error: –2.00 D) imaged by the Cirrus HD-OCT (Carl Zeiss Meditec). In the RNFL thickness map, 10 evenly spaced concentric circles with diameters ranged from 3.0 mm to 4.0 mm centered at the optic disc were superimposed and the pixels of the peak RNFL thickness (indicated by the *pink dots*) of each concentric circles were joined by two straight lines (in *red*), one along the superotemporal RNFL bundle and another along the inferotemporal RNFL bundle. The RNFL distribution angles were 103.3° (**A**) and 137.5° (**B**) and the area of abnormal RNFL measurements (in *yellow* or *red* in the RNFL thickness deviation map) were 6.49 mm² (**A**) and 0.70 mm² (**B**).

pressure, gonioscopy, and fundus examination. Subjects were excluded if they had a visual acuity worse than 20/40; clinical evidence of glaucoma (i.e., absence of visual field defects and glaucomatous optic disc changes, including neuroretinal rim narrowing, cupping, or RNFL loss detected in fundus examination); macular diseases; a history of refractive or retinal/vitreous surgeries; neurological diseases; or diabetes. The study was conducted in accordance with the ethical standards stated in the 1964 Declaration of Helsinki and approved by local research ethics committee with informed consent obtained.

Visual Field Examination

Visual field testing was performed using static automated white-on-white threshold perimetry (SITA Standard 24-2, Humphrey Field Analyzer II; Carl Zeiss Meditec). A visual field was defined as reliable when fixation losses, false-positive, and false-negative errors were less than 20%. A visual field defect was defined as having three or more significant ($P < 0.05$) nonedge contiguous points with at least one at the $P < 0.01$ level on the same side of horizontal meridian in the pattern deviation plot and confirmed with at least two consecutive

examinations. Four subjects with repeatable visual field defects were excluded.

RNFL Imaging

SD-OCT imaging was performed Cirrus HD-OCT (software version 5.1; Carl Zeiss Meditec Inc.). The details of the principles of SD-OCT have been described.[11] An "optic disc cube" scan protocol was used to measure the RNFL thickness in a 6×6 mm^2 area at the optic disc region. The RNFL thickness at each pixel was measured and an RNFL thickness map was generated. A built-in algorithm located the center of the optic disc even if it was not well-centered at the disc center.[12] The disc center was identified by finding a dark spot near the center of the scan that had a shape and size consistent with a range of optic discs. A calculation circle of 3.46 mm diameter consisting of 256 A-scans was then positioned around the optic disc and the average RNFL thickness was reported. The termination of Bruch's membrane was automatically detected as the disc margin and the optic disc area was calculated. All the OCT images had a signal strength of at least 7. Saccadic eye movement was detected in the line-scanning ophthalmoscope overlaid with OCT en face during OCT imaging. Images with motion artifact were rescanned at the same visit. RNFL segmentation was checked for every OCT image.

Measurement of the RNFL Distribution Angle in the RNFL Thickness Map

RNFL thickness data of individual pixels of the RNFL thickness map were exported to a computer for analysis via a Research Browser provided by Carl Zeiss Meditec. A computer program written using statistical software (MATLAB; MathWorks, Inc., Natick, MA) recomposed the RNFL thickness map and measured the RNFL distribution angle—that is the angle bounded by the long axes (the axes with the thickest RNFL measurements)—of the superotemporal and the inferotemporal RNFL bundles in the RNFL thickness map. To identify the long axes of the peaked RNFL thicknesses, 10 evenly spaced concentric circles with diameter ranged from 3.0 mm to 4.0 mm centered at the optic disc were superimposed on the RNFL thickness map. The long axes were defined as two straight lines extending from the optic disc center (one along the superotemporal and another along the inferotemporal RNFL bundles) toward the peaked RNFL thicknesses detected along the concentric circle so that the sum of squares of the orthogonal distance between the peaks and the axis was minimized (i.e., the principal axes in principal component analysis; Fig. 1). The selection of the ten 3 to 4 mm diameter concentric rings was arbitrary (the RNFL distribution angle may vary with the number and the size of the concentric circles selected for measurement). In this study, the same set of concentric circles with the same dimensions was applied to each of the RNFL thickness maps for measurement of the RNFL distribution angle. To evaluate the reproducibility of the measurement of RNFL distribution angle, 15 myopic eyes with a mean spherical error of –3.35 D (range: –0.75 to –5.75 D) from 15 normal volunteers (age: 33.2 ± 7.5 years, range: 26–52 years) were invited for RNFL imaging every week for 3 consecutive weeks. The coefficient of variation, reproducibility coefficient and intraclass correlation coefficient of the RNFL distribution angle were 3.60% (95% confidence interval (CI): 2.69%–4.51%); 12.59° (95% CI: 9.41°–15.78°); and 0.88 (95% CI: 0.74–0.95), respectively.

Measurement of Area of Abnormal RNFL Thicknesses in the RNFL Thickness Deviation Map

The RNFL thickness deviation map, comprising of 50×50 pixels, was generated automatically by the OCT with reference to a normative database. A pixel would be coded in yellow or red in the RNFL thickness deviation map if the RNFL measurement was below the lower 95% ("borderline") and 99% ("outside normal limits") of the centile ranges for that particular pixel, respectively. The RNFL thickness deviation maps were exported to a computer for measurement of the area of abnormal RNFL measurement.

Statistics

Statistical analyses were performed using statistical computing software (R version 2.13; R Foundation, Vienna, Austria). The associations between the RNFL distribution angle and the axial length/spherical error were analyzed with linear mixed models taking correlation between fellow eyes into account (random intercepts at the subject level). The associations between area of abnormal RNFL measurement (in the RNFL thickness deviation map) and each of the following parameters: axial length, spherical error, RNFL distribution angle, average RNFL thickness, optic disc area (measured by the OCT software [Carl Zeiss Meditec]), and signal strength were analyzed with univariate and multivariable backward selection linear mixed models taking correlation between fellow eyes into account. In the multivariable backward selection linear mixed models, axial length and spherical error were analyzed separately as they are highly correlated. After checking the model diagnostics, the assumption of normality was met in the univariate and multivariable linear mixed models when the area of abnormal RNFL thickness was defined by the lower 95th centile ranges. $P < 0.05$ was considered statistically significant.

Results

A total of 189 myopic eyes from 103 healthy participants were analyzed. The ranges of spherical error and axial length were between –0.50 and –12.50 D (mean: –5.44 ± 2.15 D), and between 23.76 and 28.84 mm (mean: 25.85 ± 0.99 mm), respectively (Table 1). No subjects had visual field defects. The angle bounded by the superotemporal and inferotemporal RNFL bundles, the RNFL distribution angle, ranged between 83.6° and 171.8°, with a mean of 121.3° ± 15.5°. There was a positive association between the RNFL distribution angle and the spherical error ($P < 0.001$, $R^2 = 0.100$), and a negative association between the RNFL distribution angle and the axial length ($P = 0.011$, $R^2 = 0.032$; Table 2, Fig. 2). For every 1-mm increase in axial length, the RNFL distribution angle decreased by approximately 3.3°. For every 1.0 D increase in spherical error, the RNFL distribution angle increased by approximately 2.6°.

The mean area in the RNFL thickness deviation map coded in red was 0.98 ± 1.03 mm^2 (range: 0.00–5.46 mm^2), representing 2.7% ± 2.9% of the total area imaged. The mean area coded in yellow or red was 2.99 ± 1.85 mm^2 (range: 0.00–9.49 mm^2), representing 8.3% ± 5.1% of the total area imaged. Figure 3 shows the frequency distribution map of the area of abnormal RNFL thicknesses in the RNFL thickness deviation map.

Table 1. Demographics, OCT Optic Disc, and RNFL Measurements

	Mean ± SD	Range
Age, y	32.0 ± 7.4	22.0 to 54.0
Spherical error, D	−5.44 ± 2.15	−12.50 to −0.50
Axial length, mm	25.85 ± 0.99	23.76 to 28.84
Average RNFL thickness, μm	90.46 ± 7.19	71.14 to 109.83
Disc area, mm^2	1.68 ± 0.32	1.09 to 2.74
RNFL distribution angle, deg	121.25 ± 15.47	83.63 to 171.75
Area coded in red in the RNFL deviation map, mm^2	0.98 ± 1.03	0.00 to 5.46
Area coded in red or yellow in the RNFL deviation map, mm^2	2.99 ± 1.85	0.00 to 9.49

SD, standard deviation.

Table 2. The Association between the RNFL Distribution Angle and the Axial Length and the Spherical Error

	Coefficient	SD	95% CI	*P*
Axial length	−3.288	1.299	−5.834 to −0.742	0.011
Intercept	205.848	33.589	140.015 to 271.681	0.000
Spherical error	2.604	0.557	1.513 to 3.696	0.000
Intercept	135.121	3.348	128.559 to 141.683	0.000

The RNFL distribution angle was fitted with fixed coefficients (fixed effects) on axial length and spherical error, with random intercepts (random effects) at the subject level to adjust for the correlation between fellow eyes.

In the univariate linear mixed models, the area of abnormal RNFL measurement (i.e., area coded in yellow or red in the RNFL thickness deviation map) was positively associated with the axial length ($P = 0.001$, $R^2 = 0.060$) and negatively associated with spherical error ($P < 0.001$, $R^2 = 0.093$); the RNFL distribution angle ($P < 0.001$, $R^2 = 0.119$); average RNFL thickness ($P < 0.001$, $R^2 = 0.247$); optic disc area ($P < 0.001$, $R^2 = 0.071$); and signal strength ($P = 0.026$, $R^2 = 0.026$; Table 3). In the multivariable backward selection linear mixed models, the area of abnormal RNFL thickness was negatively associated with the RNFL distribution angle after adjusting for axial length (Table 4), spherical error (Table 5), and other covariates. For each 10° reduction in the RNFL distribution angle, the area coded in yellow/red increased by 0.5 mm^2, or approximately 35 pixels in the RNFL deviation map, independent of the axial length or spherical error. Similar results were obtained if the myopic eyes were divided into low (spherical error: −0.5 to −3.0 D; mean: −2.32 ± 0.82 D; $n = 14$); moderate (−3.1 to −6.0 D; mean: −4.38 ± 0.90 D; $n = 109$) and high myopia (< −6.0 D; mean: −7.86 ± 1.39 D; $n = 66$; Table 6). There was no association between the degree of myopia and the abnormal area in the RNFL thickness deviation map after adjusting the effects of RNFL distribution angle, age, average RNFL thickness, and disc area.

Discussion

The significant associations between the RNFL distribution angle and the axial length/the spherical error in this study confirm our hypothesis that the superotemporal and inferotemporal RNFL bundles converge temporally with increasing degree of myopia. More important, we found that the area coded as "abnormal" in the RNFL thickness deviation map was associated the RNFL distribution angle independent of the axial length, the spherical error, and other covariates. The smaller the RNFL distribution angle, the greater the abnormal area detected in the RNFL thickness deviation map. Collectively, the distribution pattern of the RNFL bundles has a direct and significant impact on the interpretation of the RNFL map.

Quantitative analysis of the RNFL had been limited to circumpapillary measurement prior to the advent of SD-OCT.

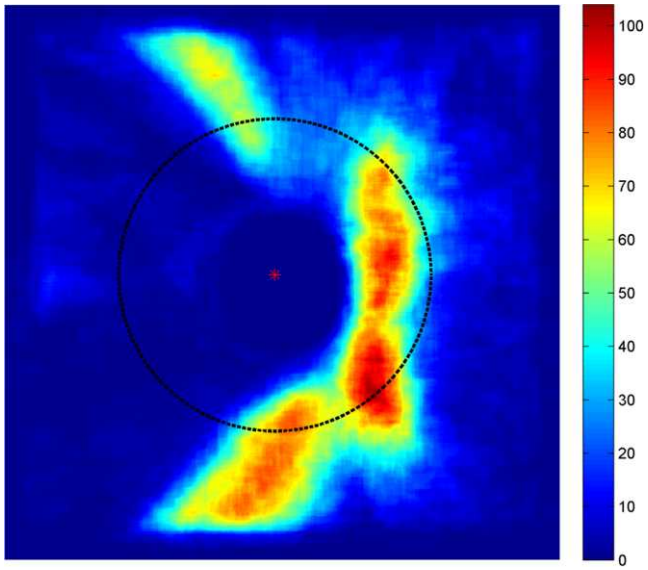

Figure 3. A frequency distribution map of the area of abnormal RNFL thicknesses (i.e., area coded in *yellow* or *red* in the RNFL thickness deviation map) was constructed by overlaying 189 RNFL thickness deviation maps from 189 myopic eyes. The color codes represent the number of eyes with abnormal RNFL thicknesses. The *red dot* represents the optic disc center, whereas the *black circle* (diameter = 3.46 mm) indicates where the measurement of average and quadrant RNFL thicknesses derived from.

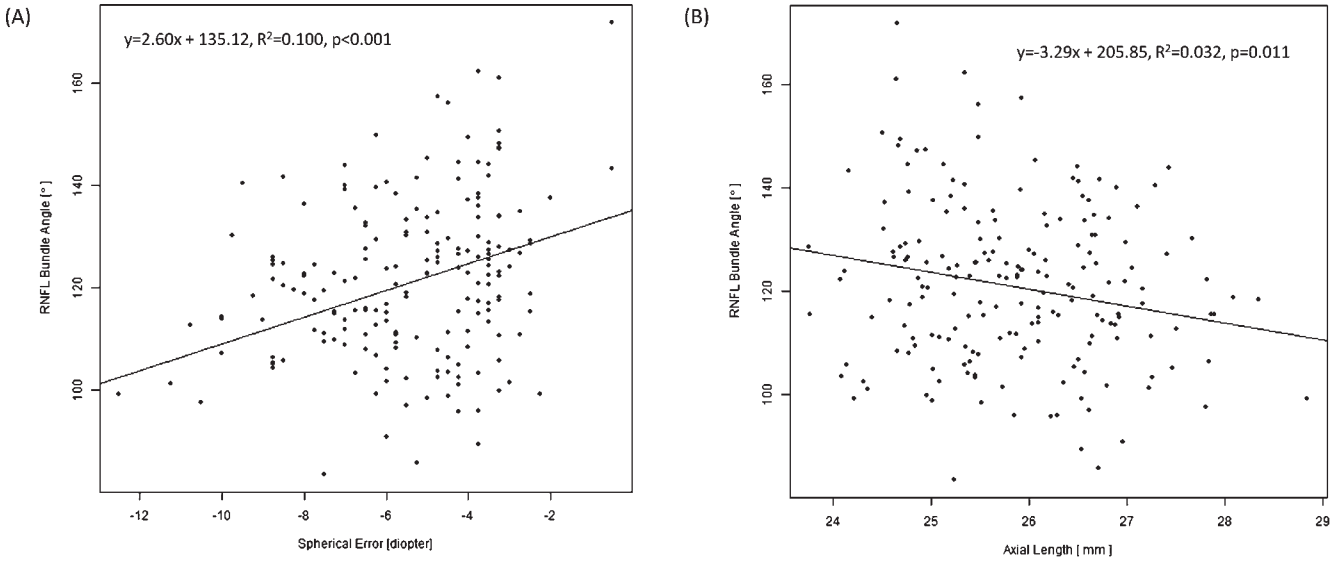

Figure 2. Scatter plots showing the relationship between RNFL distribution angle and spherical error and axial length ($n = 189$). (**A**) Spherical error ($P < 0.001$, $R^2 = 0.100$). (**B**) Axial length ($P = 0.011$, $R^2 = 0.032$).

Table 3. Univariate Linear Mixed Models Evaluating Factors Associated with the Area of Abnormal RNFL Thickness in the RNFL Thickness Deviation Map

	Coefficient	95% CI	*P*	R^2
RNFL distribution angle, deg	−0.044	−0.060 to −0.028	0.000	0.119
Axial length, mm	0.540	0.235 to 0.845	0.001	0.060
Spherical error, D	−0.297	−0.429 to −0.164	0.000	0.093
Age, y	−0.003	−0.047 to 0.042	0.904	–
Average RNFL thickness, μm	−0.139	−0.173 to −0.104	0.000	0.247
Optic disc area, mm²	−1.587	−2.392 to −0.782	0.000	0.071
Signal strength	−0.349	−0.655 to −0.043	0.026	0.026

The area of abnormal RNFL measurement was fitted with fixed coefficients (fixed effects) on each of the following: RNFL distribution angle, axial length, spherical error, age, optic disc area, average RNFL thickness, or signal strength with random intercepts (random effects) at the subject level to adjust for correlation between fellow eyes. The area of abnormal RNFL thickness is encoded in yellow or red in the RNFL thickness deviation map.

Although the distribution pattern of the RNFL cannot be fully visualized and analyzed with a circumpapillary RNFL scan, a few studies have reported that the temporal RNFL thickness was thicker in myopic eyes.[8,9] Kim et al. measured 48 myopic eyes with Stratus OCT (Carl Zeiss Meditec) and demonstrated that the temporal RNFL thickness was thicker in the moderate and high myopia (SE $\leq$ −3.0 D) group than in the low myopia group (−3.0 D $<$ SE $<$ 0.0 D).[8] Significant correlations were found between the OCT A-scan locations of the superior and inferior peaks of the double-hump RNFL profile and the axial length. In a recent study, Kang et al. measured the average and sectorial circumpapillary RNFL thicknesses in 269 young subjects (age: 19–26 years) using the Cirrus HD-OCT (Carl Zeiss Meditec).[9] Although the RNFL thickness map was not analyzed, a positive correlation between the axial length and the temporal circumpapillary RNFL thickness was noted. Likewise, Hong et al. measured the angle between the peaks of the circumpapillary RNFL profile and found a significant correlation between the angle and the degree of myopia.[13] The peaks of the RNFL thickness were closer at the temporal quadrant with increasing myopia. These studies provided preliminary data suggesting that the distribution pattern of the RNFL in myopes could be different from nonmyopes.

Visualizing the distribution of the RNFL thickness in the RNFL thickness map, we defined the long axes of the superotemporal and inferotemporal RNFL bundles, measured the angles between the RNFL bundles, and showed that this angle diminished with increasing myopia. This finding corroborates the results of the previous studies showing a positive association between temporal RNFL thickness and increasing myopia. The exact reason for the temporal convergence of the RNFL bundles is obscure, but a different globe shape in myopic eyes is in part accountable. Moriyama et al. imaged the shape of the globe in 44 eyes with high myopia

Table 4. Multivariable Backward Selection Linear Mixed Models Evaluating Factors Associated with the Area of Abnormal RNFL Thickness in the RNFL Thickness Deviation Map

Parameter	Coefficient	SD	95% CI	*P*
RNFL distribution angle, deg	−0.052	0.006	−0.065 to −0.040	0.000
Axial length, mm	0.019	0.107	−0.190 to 0.229	0.856
Age, y	−0.058	0.014	−0.087 to −0.030	0.000
Average RNFL thickness, μm	−0.154	0.015	−0.183 to −0.125	0.000
Optic disc area, mm²	−1.028	0.298	−1.612 to −0.444	0.001
Intercept	26.364	3.743	19.027 to 33.701	0.000

The area of abnormal RNFL measurement was fitted with fixed coefficients (fixed effects) on RNFL distribution angle, axial length, age, average RNFL thickness, optic disc area and signal strength with random intercepts (random effects) at the subject level to adjust for correlation between fellow eyes. Signal strength was removed after backward selection in the model fitting. The area of abnormal RNFL thickness was encoded in yellow or red in the RNFL thickness deviation map. The spherical error of the RNFL thickness map was analyzed in Table 5.

Table 5. Multivariable Backward Selection Linear Mixed Models Evaluating Factors Associated with the Area of Abnormal RNFL Thickness in the RNFL Thickness Deviation Map

Parameter	Coefficient	SD	95% CI	*P*
RNFL distribution angle, deg	−0.051	0.007	−0.064 to −0.038	0.000
Spherical error, D	−0.038	0.052	−0.140 to 0.064	0.466
Age, y	−0.060	0.015	−0.089 to −0.031	0.000
Average RNFL thickness, μm	−0.152	0.015	−0.181 to −0.123	0.000
Optic disc area, mm²	−1.007	0.299	−1.593 to −0.421	0.001
Intercept	26.332	1.953	22.504 to 30.159	0.000

The area of abnormal RNFL measurement was fitted with fixed coefficients (fixed effects) on RNFL distribution angle, spherical error, age, average RNFL thickness, optic disc area and signal strength with random intercepts (random effects) at the subject level to adjust for correlation between fellow eyes. Signal strength was removed after backward selection in the model fitting. The area of the abnormal RNFL Thickness was encoded in yellow or red in the RNFL thickness deviation map. The axial length of the RNFL thickness deviation map was analyzed in Table 4.

Table 6. Multivariable Backward Selection Linear Mixed Models Evaluating Factors Associated with the Area of Abnormal RNFL Thickness in the RNFL Thickness Deviation Map

Parameter	Coefficient	SD	95% CI	*P*
RNFL distribution angle, deg	−0.052	0.006	−0.064 to −0.039	0.000
Moderate Myopia*	0.006	0.322	−0.625 to 0.636	0.986
High myopia*	0.224	0.364	−0.490 to 0.938	0.538
Age, y	−0.061	0.015	−0.089 to −0.032	0.000
Average RNFL thickness, μm	−0.152	0.015	−0.180 to −0.123	0.000
Optic disc area, mm²	−1.022	0.298	−1.607 to −0.437	0.001
Intercept	26.541	1.862	22.892 to 30.190	0.000

The area of abnormal RNFL measurement was fitted with fixed coefficients (fixed effects) on RNFL distribution angle, myopia classification, age, average RNFL thickness, optic disc area and signal strength with random intercepts (random effects) at the subject level to adjust for correlation between fellow eyes. Signal strength was removed after backward selection in the model fitting. The area of abnormal RNFL thickness was encoded in yellow or red in the RNFL thickness deviation map. Eyes were classified into low (spherical error: −0.5 to −3.0 D); moderate (−3.1 to −6.0); and high myopia ($<$ −6.0 D).

* The coefficients were derived from the comparison with low myopia. The comparison between moderate and high myopia was insignificant ($P = 0.302$).

(≤ -8.0 D or axial length >26.5 mm) using a high-resolution MRI with volume-rendering techniques.[14] They showed that while emmetropic eyes are consistently spherical, myopic eyes demonstrated symmetrical or asymmetrical anteroposterior elongation and posterior protrusions. It is plausible that the distribution of the RNFL bundles conforms to the shape of the globe. An asymmetrical anteroposterior elongation or a posterior protrusion could draw the superior and inferior RNFL bundles closer to the macula. Alternatively, the temporal convergence of the RNFL bundles could be an image artifact consequential to an increase in the vertical curvature of the retina. The bending at the posterior protrusion may create an impression of temporal convergence of the superior and inferior RNFL bundles, artificially reducing the angle between the superotemporal and inferotemporal RNFL bundles when it is visualized in a fundus image.

Regardless of the underlying cause, the different RNFL distribution pattern in myopic eyes already has important implications in the interpretation of the RNFL thickness map. The significant negative association between the area of abnormal RNFL measurement and the RNFL distribution angle, even after adjustment of axial length/spherical error, signifies that the built-in normative database would not be suitable to analyze RNFL thickness measurements in eyes with a small RNFL distribution angle. Notably, the analysis software would not be able to recognize the temporal convergence of the RNFL bundles, rendering RNFL measurement pixels nasal to the superotemporal and inferotemporal RNFL bundles labeled as "borderline" or "outside the normal limits" (Fig. 1A). These abnormal RNFL pixels should not be considered as glaucomatous RNFL defects.

The significant association between the area of abnormal RNFL thickness and the average RNFL thickness in the univariate and multivariate analyses is expected, although the origin of the negative association with optic disc area is less certain. With time-domain OCT RNFL measurement, it has been shown that the average RNFL thickness is positively correlated with optic disc size.[15,16] Similarly, in a recent study analyzing Cirrus HD-OCT circumpapillary RNFL measurement, myopic eyes with a small disc area were associated with an increased propensity for an abnormal diagnostic classification.[10] While the decrease in RNFL thickness and the increase in abnormal diagnostic classification in eyes with a small optic disc have been attributed to the decreasing circumpapillary RNFL thickness with increasing distance away from the optic disc margin, the negative association between the area of abnormal RNFL measurement and optic disc area after adjusting for other covariates suggests that a smaller optic disc may have fewer nerve fibers and a thinner RNFL.[17,18]

It is worth noting that the RNFL distribution angle derived from this study only provides a surrogate measure of the RNFL distribution profile. The trajectory of the superotemporal and inferotemporal RNFL bundles is curvilinear, arching from the optic disc toward the macula. The angle between the major linear axes of the RNFL bundles only approximates, but would not represent the complete RNFL trajectory. Nevertheless, the RNFL distribution angle defined in this study facilitates the evaluation of the RNFL distribution profile and its association with myopia and interpretation of the RNFL thickness deviation map.

To summarize, the RNFL distribution angle diminished with increasing myopia and this reduction could lead to abnormal RNFL measurement in the RNFL thickness deviation map. Even though the current software of the Cirrus HD-OCT (Carl Zeiss Meditec) has not allowed measurement of the RNFL distribution angle, nor has it included a normative database for moderate and high myopic eyes, clinicians can always evaluate the RNFL thickness deviation map with reference to the RNFL thickness map to minimize the probability of labeling a normal myopic eye as glaucomatous. By examining the distribution pattern of the RNFL thickness and its symmetry in the superior and inferior quadrants in the RNFL thickness map, it is feasible to determine if the abnormal RNFL measurement pixels in the RNFL deviation map are related to a small RNFL distribution angle. This study shows that the interpretation of the RNFL measurements in myopic eyes requires careful consideration of the RNFL distribution angle. An "abnormal" RNFL thickness deviation map may not indicate the RNFL measurements are outside the normal ranges in the presence of a small RNFL distribution angle.

References

1. Kang SY, Sung KR, Na JH, et al. Comparison between deviation map algorithm and peripapillary retinal nerve fiber layer measurements using Cirrus HD-OCT in the detection of localized glaucomatous visual field defects. *J Glaucoma*. 2012;21:372–378.
2. Savini G, Carbonelli M, Barboni P. Spectral-domain optical coherence tomography for the diagnosis and follow-up of glaucoma. *Curr Opin Ophthalmol*. 2011;22:115–123.
3. Leung CK, Lam S, Weinreb RN, et al. Retinal nerve fiber layer imaging with spectral-domain optical coherence tomography: analysis of the retinal nerve fiber layer map for glaucoma detection. *Ophthalmology*. 2010;117:1684–1691.
4. Leung CK, Choi N, Weinreb RN, et al. Retinal nerve fiber layer imaging with spectral-domain optical coherence tomography: pattern of RNFL defects in glaucoma. *Ophthalmology*. 2010; 117:2337–2344.
5. Leung CK, Mohamed S, Leung KS, et al. Retinal nerve fiber layer measurements in myopia: an optical coherence tomography study. *Invest Ophthalmol Vis Sci*. 2006;47:5171–5176.
6. Vernon SA, Rotchford AP, Negi A, et al. Peripapillary retinal nerve fibre layer thickness in highly myopic Caucasians as measured by Stratus optical coherence tomography. *Br J Ophthalmol*. 2008;92:1076–1080.
7. Rauscher FM, Sekhon N, Feuer WJ, et al. Myopia affects retinal nerve fiber layer measurements as determined by optical coherence tomography. *J Glaucoma*. 2009;18:501–505.
8. Kim MJ, Lee EJ, Kim TW. Peripapillary retinal nerve fibre layer thickness profile in subjects with myopia measured using the Stratus optical coherence tomography. *Br J Ophthalmol*. 2010; 94:115–120.
9. Kang SH, Hong SW, Im SK, et al. Effect of myopia on the thickness of the retinal nerve fiber layer measured by Cirrus HD optical coherence tomography. *Invest Ophthalmol Vis Sci*. 2010;51:4075–4083.
10. Qiu KL, Zhang MZ, Leung CK, et al. Diagnostic classification of retinal nerve fiber layer measurement in myopic eyes: a comparison between time-domain and spectral-domain optical coherence tomography. *Am J Ophthalmol*. 2011;152:646–653.
11. Nassif N, Cense B, Park BH, et al. In vivo human retinal imaging by ultrahigh-speed spectral-domain optical coherence tomography. *Opt Lett*. 2004;29:480–482.
12. Cirrus HD-OCT user manual. *Rev. A*. Dublin, CA: Carl Zeiss Meditec Inc.; 2008;4-18–9.
13. Hong SW, Ahn MD, Kang SH, et al. Analysis of peripapillary retinal nerve fiber distribution in normal young adults. *Invest Ophthalmol Vis Sci*. 2010;51:3515–3523.
14. Moriyama M, Ohno-Matsui K, Hayashi K, et al. Topographic analyses of shape of eyes with pathologic myopia by high-resolution three-dimensional magnetic resonance imaging. *Ophthalmology*. 2011;118:1626–1637.

15. Budenz DL, Anderson DR, Varma R, et al. Determinants of normal retinal nerve fiber layer thickness measured by Stratus OCT. *Ophthalmology.* 2007;114:1046–1052.
16. Savini G, Zanini M, Carelli V, et al. Correlation between retinal nerve fibre layer thickness and optic nerve head size: an optical coherence tomography study. *Br J Ophthalmol*. 2005; 89:489–492.
17. Jonas JB, Müller-Bergh JA, Schlötzer-Schrehardt UM, Naumann GO. Histomorphometry of the human optic nerve. *Invest Ophthalmol Vis Sci*. 1990;31:736–744.
18. Quigley HA, Coleman AL, Dorman-Pease ME. Larger optic nerve heads have more nerve fibers in normal monkey eyes. *Arch Ophthalmol*. 1991;109:1441–1443.